ISIJ International, Vol. 47 (2007), No. 2, pp. 226–233

In Situ Observation of Reduction Behavior of Hematite with Solid Carbon and Crystallographic Orientation between Hematite and Magnetite

Yoshiaki KASHIWAYA,[1)] Yasuhide YAMAGUCHI,[2)] Hiroshi KINOSHITA[1)] and Kuniyoshi ISHII[3)]

1) Graduate School of Engineering, Hokkaido University, Kita-ku, Kita 13-jo, Niishi 3-chome, Sapporo 060-8628 Japan.
2) Formerly Graduate School of Engineering, Hokkaido University. Now at Sumitomo Metal, Co. Ltd.
3) Professor Emeritus, Hokkaido University. Now Advisor of JFE Steel Corp., Kawasaki-cho, Chuo-ku, Chiba 260-0835 Japan.

(*Received on July 26, 2006; accepted on October 24, 2006*)

Recently, the composite pellets between iron ore and carbon are studied by many researchers because of its high reactivity. However, the reaction mechanism of the composite pellet is not yet clarified. It is obviously determined the reaction mechanism at initial stage as the direct reaction between solid carbon and iron oxide. However, in the course of reaction, the reaction mechanism will change to the indirect reduction of iron oxide with CO gas owing to the separation of the interface between solid carbon and iron oxide.

In this study, samples of polycrystalline hematite (grain size was approximately 20 μm) were prepared. The hematite sample was coated by carbon with different thickness. The *in situ* observation by a laser microscope was carried out. The crystal orientation and morphology was investigated before and after the reaction using EBSP, SEM, AFM, XRD and Raman.

The direct reduction began from about 650°C and the reaction proceeded rapidly until carbon was consumed. The behavior of reduction was different from the thickness of carbon layer (amount of carbon) which was related to whether the product gas (CO) could be passed through the carbon layer or not. After reduction, the lath magnetite having same direction was a grain was observed on the surface. The crystallographic orientation between magnetite and hematite was as follows;

$$(0\,0\,0\,1)_H \parallel (1\,1\,1)_M, \quad [1\,\bar{1}\,0\,0]_H \parallel [1\bar{1}0]_M$$

In addition, the growth direction of the lath magnetite formed on the hematite surface was

$$[2\,1\,\bar{3}\,0]_H \parallel [10\bar{1}]_M$$

KEY WORDS: direct reduction; iron oxides; EBSP; crystallographic orientation; carbon composite.

1. Introduction

The responsibility of all industries for reducing the CO_2 emission after Kyoto protocol (COP3: The 3rd Session of the Conference of the Parties to the United Nations Framework Convention on Climate Change, http://unfccc.int) are more and more increasing. Especially for iron and steelmaking industries in Japan, in which quite high efficiency is already attained, the amount of carbon usage is very large in comparison with other industries. From this reason, it would be possible to perform the most effective reduction of CO_2 emission in iron and steel industry. Furthermore, rapidly growing of NICs(Newly Industrializing Countries) that has no obligation to undertake the COP3 assignation have a actual and powerful effect on the reduction of CO_2 in terms of ironmaking process.

Anyway, it is important for ironmaking process to reduce the energy (CO_2 emission). In order to clear this problem, many investigations in iron and steel making process in Japan are carried out. Recently, the composite pellets between iron ore and carbon are studying by many researchers, because of its high reactivity and relatively lower reaction temperature. However, the reaction mechanism occurring in the composite pellet is not yet clarified. For example, the reaction of the composite pellet can occur even in an inert atmosphere. It is obviously determined the reaction mechanism at initial stage as the direct reaction between the solid carbon and the iron oxide (Eq. (1)).

$$Fe_xO_y + C = Fe_xO_{y-1} + CO \quad \ldots\ldots(1)$$

However, in the course of reaction, the reaction mechanism will change to the indirect reduction of iron oxide with CO gas owing to the separation of the interface between the solid carbon and the iron oxide (Eq. (2)).

$$Fe_xO_y + CO = Fe_xO_{y-1} + CO_2 \quad \ldots\ldots(2)$$

And in this case, the rate limiting step will be in the gasification of the carbonaceous materials with CO_2 (Boudouard

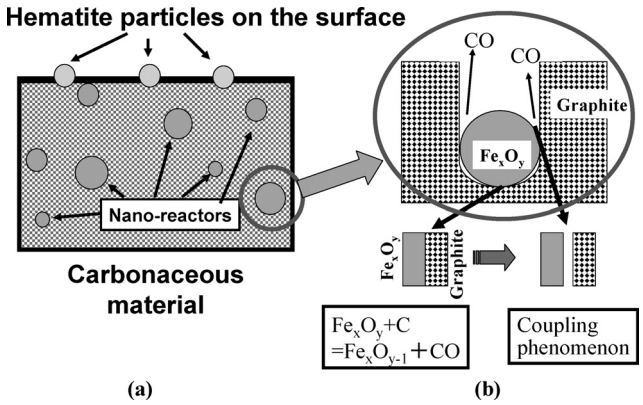

Fig. 1. Illustration of Nano-reactior and reactions : direct reaction between iron oxide and solid carbon, and coupling phenomenon.

reaction) (Eq. (3)), that the most of researchers have determined in their studies.

$$C+CO_2=2CO \quad \text{.....(3)}$$

Recently, reaction behaviors on a nano-reactor consisted of hematite and graphite, which was made by a mechanical milling, were reported.[1–3] A good contact in atomic level between iron oxide and carbon was attained by the milling, and both of quite high rate of reduction and lower reaction temperature (~650°C) were obtained under an inert atmosphere. In such a sample, hematite was not only becoming a fine particle but also intruding into carbonaceous material, which formed a so called nano-reactor. The ideal image of nano-reactors are shown in **Fig. 1**(a) and the behavior of the each reactor's reaction has been presented as shown in Fig. 1(b). The basic reaction mechanism of nano-reactor will be the same as the above mentioned composite pellet, that is, the initial reaction is caused by the direct contact between the iron oxide and the carbon, and the subsequent reaction after the separation of the interface is the coupling phenomenon between the reduction and the gasification reaction.[4] However, in the case of nano-reactor, the intensities of respective reactions would be different and the overall reaction rate could ultimately increase owing to the tight contact in atomic level.

Until now, many investigations related to the reduction of hematite to magnetite with CO and H_2 gases have been conducted.[5–16] However, direct reduction with a solid carbon was not carried out and no consideration of crystallographic orientation was conducted. Furthermore, there is little publication on the *in situ* observation of the reaction and its mechanism between solid carbon and iron oxide.

On the other hand, microscopic investigations in the course of reduction reaction by gases (H_2 or CO) were studied by means of SEM and TEM.[5–10] The crystallographic orientation between hematite and magnetite by means of H_2 implantation was reported by Watanabe *et al.*[10]

In this study, solid carbon was deposited on the iron oxide surface. The initial stage of mechanism on the direct reaction was observed directly by a laser microscope. In addition, the product on the surface after experiment was examined by XRD and Raman spectroscopy. Furthermore, the morphology changed after the reaction was observed by SEM and AFM, and the crystal orientation between hematite and magnetite was clarified by EBSP.

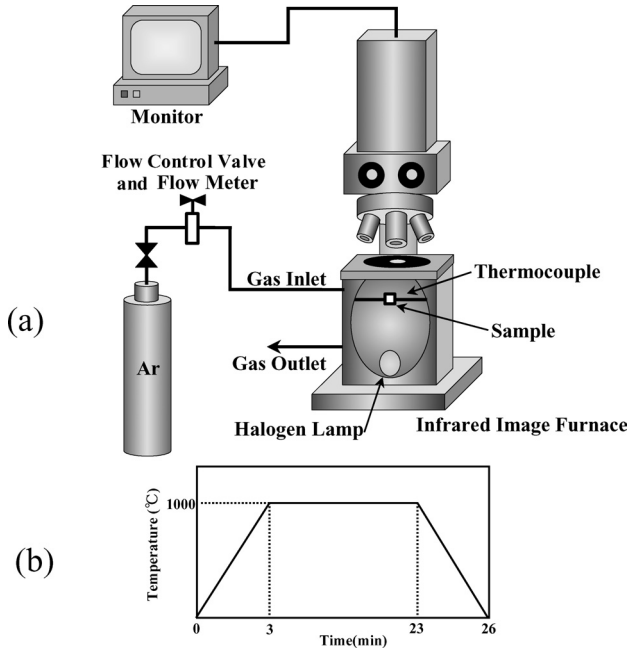

Fig. 2. (a) Schematics of experimental apparatus (high temperature laser microscope) and (b) heat pattern of experiment.

2. Experimental

In this study, a sample consisted of poly crystalline hematite was used. Regent grade hematite was pressed into a tablet with 200 kgf/cm^2. The tablet was sintered in a muffle furnace at 1 100°C for 120 h to grow the large grain (average grain size was 20 μm). The sintered tablet was cut into small pieces (about 5×5×2 mm) and the surface for observation was polished with SiC paper, diamond paste and colloidal SiO_2.

Before the carbon coating on the sample surface was carried out, the surface characteristics were observed and measured by SEM and EBSP. Moreover, Raman Spectroscopy was also carried out in some sample.

Then, the sample was coated by carbon with vacuum deposition method. The thicknesses of carbon deposition were changed to three levels, 20 nm (Sample-1), 60 nm (Sample-2) and 300 nm (Sample-3), which were controlled by the length and diameter of carbon rod for evaporation. Those carbon thicknesses were examined by SEM after embedding in a resin and cutting in a cross section for test samples.

The carbon-coated sample was put on an alumina crucible (5 mmϕ) and heated up to the desired temperature in the IR (Infra red) image furnace equipped with the laser microscope as shown in **Fig. 2**(a). The *in situ* observation by the laser microscope was carried out under high purity Ar atmosphere (P_{O_2}<0.1 ppm, 500 Ncc/min) using the heating program that a heating up rate was 5.56°C/s until 1 000°C and held for 10 min at 1 000°C (Fig. 2(b)). The image during experiment was recorded on the DVD and the image processing was carried out for analyzing the reaction behavior after experiment.

In addition, the morphology and the crystallographic orientation of grains on the surface of sample were also ob-

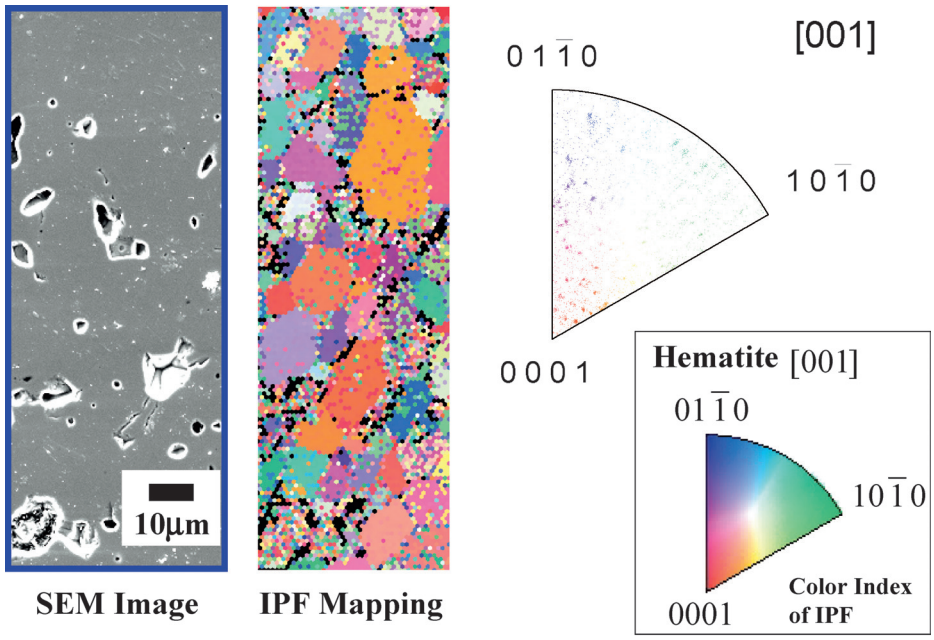

Fig. 3. Results of SEM and EBSP observations of hematite before experiment.

served and measured by SEM, EBSP and AFM as well as before experiment. It is important to note the detail of experiment that the same position in the sample should be found after experiment. For attaining to this purpose, a micro-Vickers was used and some markers of Vickers were put on the sample surface before the carbon coating for identifying the same position after experiment easily.

3. Results and Discussions

3.1. *In Situ* Observation by Laser Microscope

Figure 3 shows the typical example of SEM observation and EBSP measurement of hematite sample without carbon coating before experiment. In the case of SEM observation, it was difficult to distinguish the grain. Only the position of pore and/or the surface defect could identify the same position with the result of EBSP, so that the marker of micro-Vickers assisted to find the same position (In Fig. 3, a maker of micro-Vickers could not see in the area and it was just located near the observation area). The average size of grain was found to be about 5 to 20 μm from the EBSP. The crystallographic orientation of grains showed a relatively uniform distribution in a short time of heat treatment ($<$120 h), however, the orientations of the grains seemed to be gradually changed to [1 0 $\bar{1}$ 0] during the heat treatment at 1 150°C. Finally, it was seemed to assort with a plane (0 0 0 1) of hematite, if longer time of heat treatment was carried out. However in this experiment, as the maximum temperature was 1 000°C, the change (or growth) of hematite grains did not occur after experiment.

Figures 4–6 show the results of *in-situ* observation by the laser microscope, which were recorded on the DVD and the still images were captured. Figure 4 shows the result of *in situ* observation of hematite-carbon direct reaction for the sample-1 with the carbon thickness of 20 nm. The reaction started from about 650°C (Fig. 4(b), 648°C, 117 s). A corrugation structure formed on the surface in the course of reaction, which would be caused by the reduction reaction

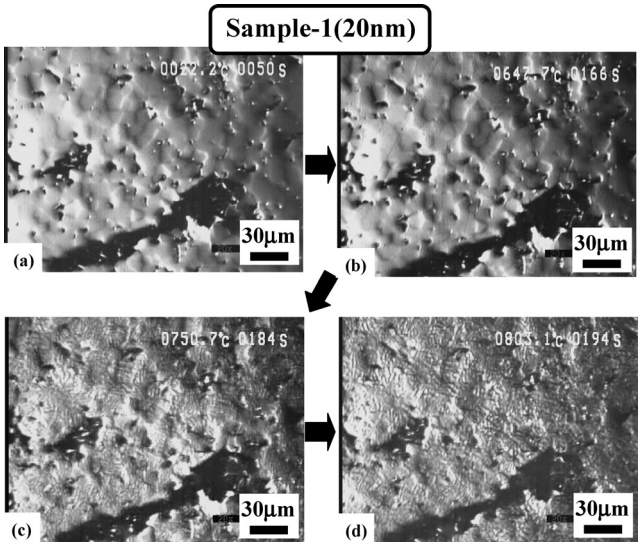

Fig. 4. Change of microstructures of Sample-1 (carbon thickness; 20 nm) during experiment. (a) room temp., 1 s, (b) 648°C, 117 s, (c) 751°C, 135 s, (d) 803°C, 145 s.

(the shrinkage of hematite by the removal of oxygen and the formation of lath magnetite; the details will be mentioned below.). Finally, the reaction proceeded rapidly around 750°C (Fig. 4(c), 751°C, 135 s) and finished within 10 s (Fig. 4(d), 803°C, 145 s). After 30 s, there was no change on the surface during the holding at 1 000°C. It was considered that all deposited carbon on the hematite sample was consumed by the direct reduction (Eq. (1)).

Sample-2 (60 nm, Fig. 5), which was a middle thickness of carbon, also began to change from 646°C (Fig. 5(b)). However, the difference from the Sample-1 was the formation of the bubble-like structure arose from surface. It was thought that the CO gas generated by the direct reduction (Eq. (1)) at the interface between the hematite and the carbon, and the carbon film was pushed up by the gas produced. The number of bubble increased drastically within

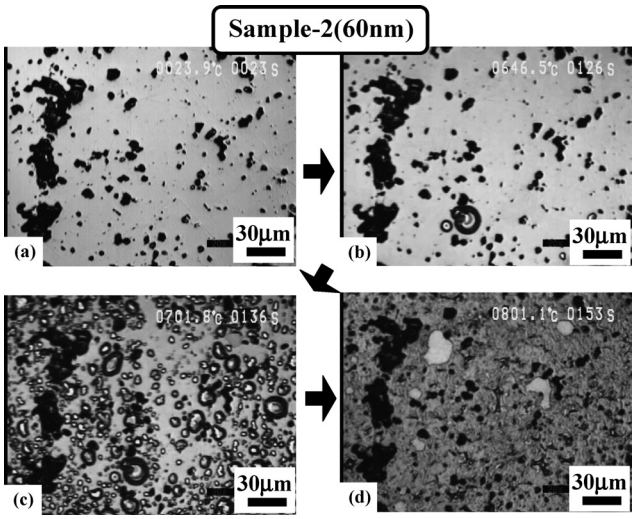

Fig. 5. Change of microstructures of Sample-2 (carbon thickness; 60 nm) during experiment. (a) room temp., 13 s, (b) 646°C, 116 s, (c) 702°C, 126 s, (d) 801°C, 143 s.

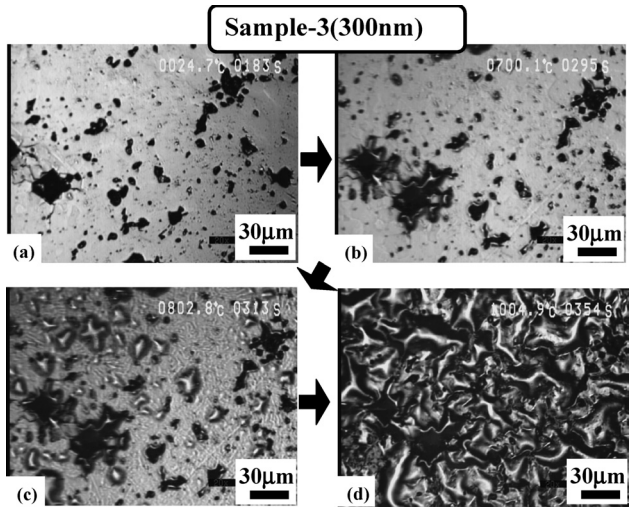

Fig. 6. Change of microstructures of Sample-3 (carbon thickness; 300 nm) during experiment. (a) room temp., 14 s, (b) 700°C, 126 s, (c) 803°C, 144 s, (d) 1005°C, 185 s.

10 s from 646°C (Fig. 5(b) to 701°C (Fig. 5(c)). The remained carbon film, which located at the edge of bubbles, maintained a contact with hematite and continued to react (Fig. 5(c)). There was a hole to escape the produced gas, which was caused to finish growing the bubbles, although an overall reaction was still continuing. Finally, the reaction itself finished in about 30 s (800°C, Fig. 5(d)) because of lack of carbon as well as Sample-1.

Figure 6 shows the results of the experiment using Sample-3 (300 nm). It was found that the temperature of the beginning of reaction was about 700°C (Fig. 6(b)). It was close to the results of other two samples. As it is difficult to find the beginning of reaction owing to the thick carbon layer, the exact temperature of the reaction start will be lower than 700°C and the same as other samples. In addition, the evolved CO gas was difficult to pass through the carbon layer, larger bubbles were formed on the sample surface (Fig. 6(c); 803°C, (d); 1 005°C) and propagated through channels which seemed to a mountains on the surface (Fig. 6(d)). Then, because of the larger bubbles, the

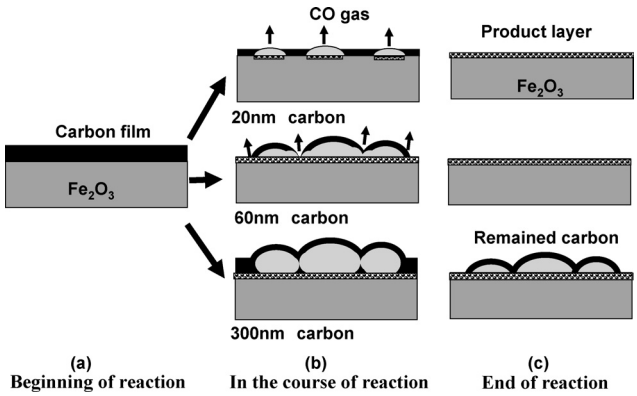

Fig. 7. Schema of reaction processes of samples with different carbon thickness.

contact between hematite and carbon was disturbed and the reaction never occur at Fig. 6(d), even in the maximum temperature (1 005°C).

These reaction processes were summarized in **Fig. 7**. In accordance with the difference of the thickness of carbon layer, reaction behaviors were quite different, which was caused by the product gas. When the evolved gas can be passed through the carbon layer, the continuous contact between iron oxide and carbon can be maintained, and the direct reduction can be continued until the carbon was consumed (Figs. 7(a), 7(b)). While the evolved gas can not pass the carbon layer, carbon bubbles were formed on the surface and reaction between solid carbon and hematite is finished. However, there will be an apparent direct reaction consisted of Eq. (2) and Eq. (3) occurring within the bubbles, in which a coupling phenomenon would occur.[4)]

Although there was a remained carbon after experiment in the case of thickest layer (300 nm), the total amount of reaction was largest, that was qualitatively found from the results of XRD and Raman spectroscopic analysis. Especially, the height of the produced structure (lately lath magnetite) by AFM increased with the increase of carbon thickness, however, the quantitative discussion for the magnetite formation was difficult with the result of XRD, Raman and AFM. The gas analysis of the exhausted gas will be best method to clarify the quantity of the reduction degree. Furthermore, the content of CO_2 in the exhausted gas will clarify the extent of indirect reaction, Eq. (2), which related to the reaction mechanism inside the bubble. In present experiment, the gas analysis of the exhausted gas was impossible, because the laser microscope could not modify. New high temperature microscope having gas analysis device (QMS: Quadrupole mass spectrometer) will be prepared by the authors and the results will be published in the future.

3.2. Morphology of Surface after Reaction and the Analyses (XRD and Raman) of Surface Product

Figure 8 shows the result of SEM observation for the Sample-3 (300 nm) before and after experiment. There are relatively many pores around 1 to 5 μm on the sample surface before experiment (Fig. 8(a) and Fig. 3). The appearance of the surface just after experiment seemed that shown in Fig. 6(d) where a remained carbon film covered the surface. However, the residual carbon film was easily removed during a handling of sample and the product layer formed

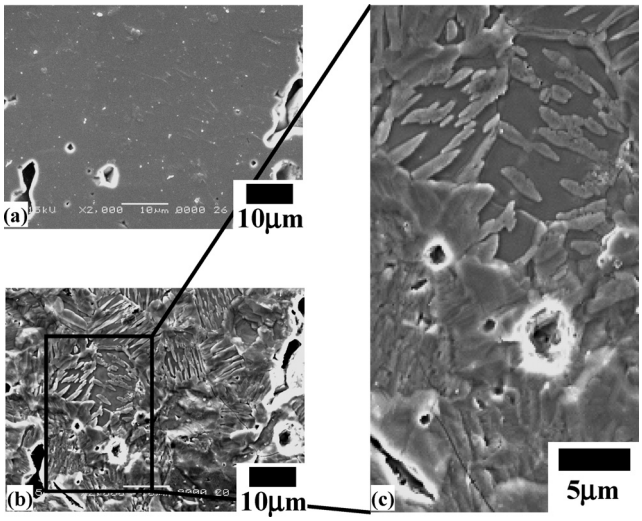

Fig. 8. Microstructure of Sample-3 (300 nm) after experiment.

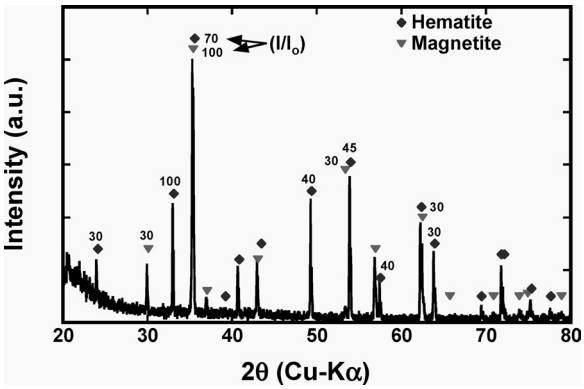

Fig. 9. Results of XRD analysis after experiment (60 nm).

on the hematite surface appeared like Fig. 8(b). After experiment, it was observed that a lath structure (1 μm width and 5–10 μm length) formed on the surface, which had the same direction within a same grain. The number of the lath structure was different from the different grain. Some of grain was filled with the lath and other grain had a few lath, so that the whole shape of the single lath structure having same direction could be seen.

The larger magnification of the area enclosed by rectangle is shown in Fig. 8(c). It was found that the adjacent two grains was located in the upper part of Fig. 8(c) and the each grain had a different direction of the lath structure.

To examine the lath structure, XRD analysis and Raman spectroscopy were carried out. At first, XRD analysis was carried out to clarify the product on the surface. As the sample size was small and about 5×5 mm, the XRD setup (Debye–Scherrer method) equipped with a sample rotation system was used to detect the small amount of product formed on the surface. The result of XRD for the sample-2 (carbon thickness of 60 nm) is shown in **Fig. 9**. The intense peaks from magnetite were found among the ones of hematite. The numbers written on the peaks means the relative intensities (I/I_0) of hematite and magnetite (◆: Hematite, ▼: Magnetite). There was a tendency to increase the magnetite with the increase of carbon thickness.

Since the XRD brings an information of relatively deep and wide region of the surface, it was difficult to examine

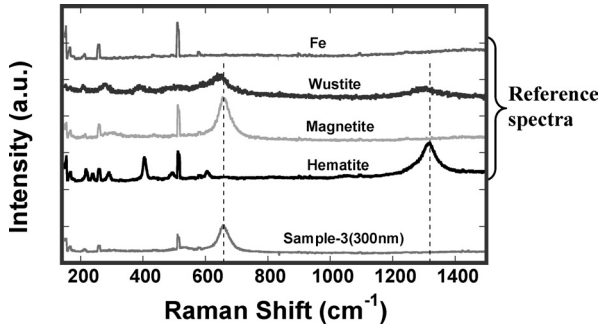

Fig. 10. Results of Raman Spectroscopy of Sample-3 (300 nm).

the lath itself on the surface. Then, Raman spectroscopy was carried out, because the laser gave an information of a shallow (<100 nm) and narrow (<1 μm) region[17] in the surface and the distance resolution was about 100 μm. The measurement was carried out on the area of Fig. 8(b) and the result was shown in **Fig. 10** in comparison with the reference data, that are metallic iron (Fe), Wustite (Fe_tO), Magnetite (Fe_3O_4) and Hematite (Fe_2O_3). Those reference samples were made by authors using an electric furnace with the atmosphere (CO/CO_2 or air) controlled reaction tube. It was found that the product layer on the sample consisted of magnetite and there was no hematite on the surface in the cases of 60 nm and 300 nm thicknesses of carbon. On the other hand, the spectra of hematite were found in the intense spectra of magnetite for the 20 nm carbon thickness, although the result was not shown.

From these result, it could be concluded that the lath structure formed on the surface was magnetite and could be called as a 'lath magnetite', hereinafter.

To clarify the crystallographic orientation between the hematite and the lath magnetite, EBSP analysis was carried out on the area shown in Fig. 8. The results of EBSP analyses before and after experiment were shown in **Fig. 11**. After experiment, the respective lath magnetites formed in the same grain showed the same color (same orientation). Index color of IPF (Inverse Pole Figure) was also shown in Fig. 11. When the results of the analyses were focused on the two grains expressed by yellow and orange (g1 and g2), it was found that the lath magnetite was almost the same direction within a grain, however, the lath magnetites between two grains showed a different direction. The details of orientation were shown in **Fig. 12**. The grain g1 showed the orientation of hematite, $(2\,\bar{9}\,7\,23)_H$, $\langle\bar{7}\,\bar{5}\,12\,\bar{5}\rangle_H$. In this case, the directions of $[0\,0\,0\,1]_H$ and $[1\,\bar{1}\,0\,0]_H$ are expressed by blue and red arrows, respectively. The lath magnetite formed on the grain g1 showed the orientation of magnetite, $(\bar{3}\,\bar{1}\,10)_M$, $\langle\bar{1}\,\bar{1}\,7\,\bar{2}\rangle_M$. The elemental directions, $[111]_M$, $[10\bar{1}]_M$ and $[1\bar{1}0]_M$ are expressed by blue, green and red, respectively. Similarly, the orientation of grain g2 was $(\bar{2}\,3\,\bar{1}\,16)_H$, $\langle 28\,\bar{1}7\,\bar{1}1\,6\rangle_H$. The lath magnetite formed on the g2 was $(\bar{1}2\,\bar{7}\,24)_M$, $\langle 1\,\bar{1}2\,\bar{3}\rangle_M$. As a result, the direction of $[0\,0\,0\,1]_H$ is parallel to $[111]_M$, accordingly, plane $(0\,0\,0\,1)_H$ is parallel to $(111)_M$.

From the crystallographic orientation of hematite and magnetite, it was found the relationship of plane orientation is as follows,

$$(0\,0\,0\,1)_H \parallel (111)_M \quad \text{.....(4)}$$

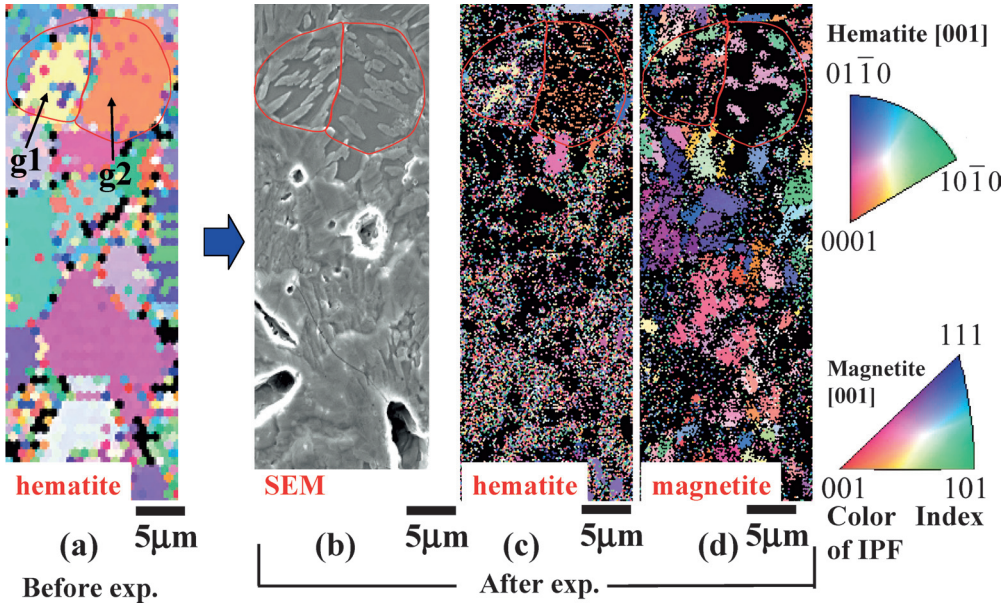

Fig. 11. Results of EBSP analyses of Sample-3 (300 nm) before and after experiment.

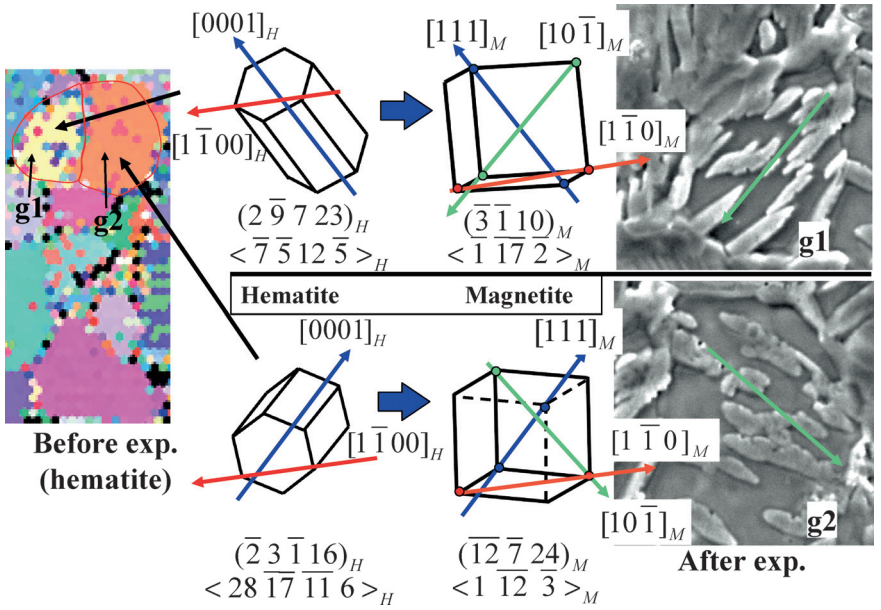

Fig. 12. Relationship of crystal orientation between hematite and magnetite formed.

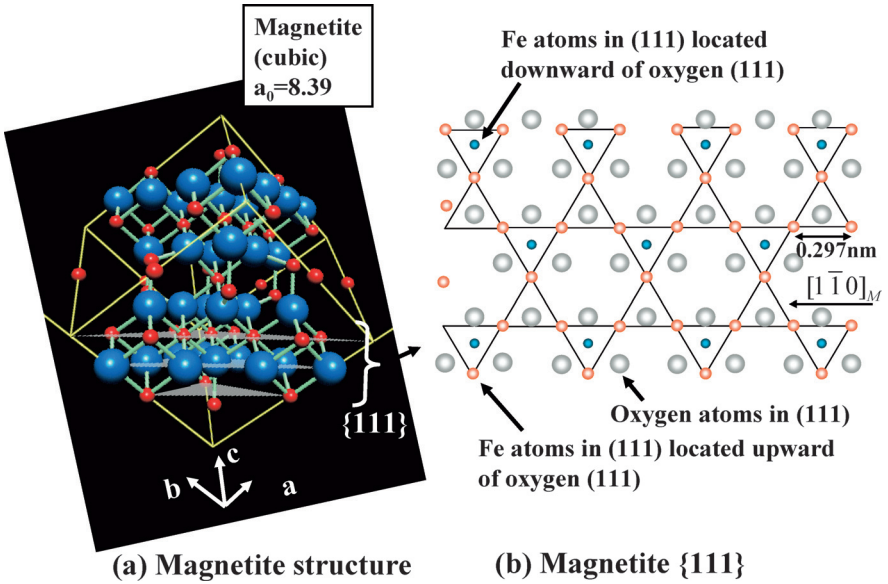

Fig. 15. Illustration of Magnetite structure (a) and projection of {111} to one sheet.

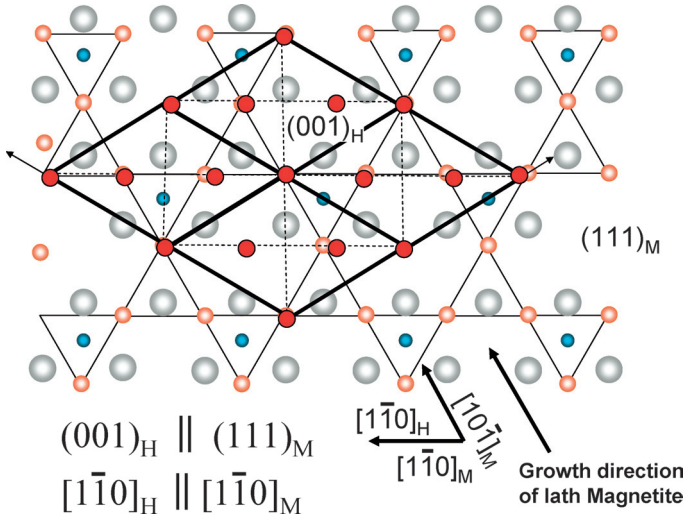

Fig. 16. Crystallographic orientation between hematite and magnetite. And relationship between (001) of hematite and (111) of magnetite.

which is the same orientation with Watanabe *et al*.[10] and other researchers.[6–9] However, the directional orientation in the present study was different from Watanabe *et al*. ($[1\,0\,\bar{1}\,0]_H \parallel [1\,\bar{1}\,0]_M$), and as follows,

$$[1\,\bar{1}\,0\,0]_H \parallel [1\bar{1}0]_M \quad \text{(present study)} \quad \text{.....(5)}$$

Those orientations of direction between the result of Watanabe *et al.* and the present study are very close (the details are shown in Fig. 16). It would caused by the difference of the two reaction systems (H_2 implantation and direct reduction with solid carbon).

In addition to the crystallographic orientation, it is interesting to note that the relationship of the direction of the growth of the lath magnetite is as follows;

$$[2\,1\,\bar{3}\,0]_H \parallel [10\bar{1}]_M$$
$$\text{(growth direction of lath magnetite to hematite)} \quad \text{.....(6)}$$

which is the same direction obtained by Hayes *et al*.[8]

To confirm these orientations, atom alignments on $\{001\}_H$ and $\{111\}_M$ were examined as shown in **Figs. 13** to **16**. Hematite structure is expressed both with trigonal and hexagonal. Hereinafter, the trigonal system was adopted for the consideration of the transformation from hematite to magnetite. The size of unit cell is a_0=5.036 Å and c_0=13.749 Å (α=90°, β=90°, γ=120°). In Fig. 13, eighteen planes paralleled to $\{001\}_H$ were shown. The values of c written in Fig. 13 are fractional coordinate of c ($=c_i/c_0$). When the first four planes from c=0.022 to c=0.189 were taken into account of the transformation from hematite to magnetite according to the reduction, iron atoms come into one plane, which is shown in Fig. 14. From the crystallographic orientation obtained from EBSP analysis (Fig. 12), $(001)_H$ shown in Fig. 14(b) will parallel to the $(111)_M$ of Magnetite. In Fig. 15, three of $\{111\}_M$ in the magnetite structure (Fig. 15(a)) and the projection into one plane of $\{111\}_M$ (Fig. 15(b)) are shown. The alignment of Fe atoms in the direction of $[1\bar{1}0]_M$ is high density and the distance of Fe atoms is 0.297 nm. On the other hand, the distance of Fe atoms in the $[1\bar{1}0]_H$ is 0.290 nm (Fig. 14(b)) which is very close value to the magnetite one.

In Fig. 16, Hematite $(001)_H$ is superposed on the projected Magnetite $(111)_M$. From this operation, the movement of Fe atoms can be minimized. However, this relationship might be dominant on the surface reaction of hematite occurring in the present study, because transformation in the bulk obtained by Watanabe *et al.* would be more complicated macroscopically.

Then, the surface morphology change after reaction was measured by means of AFM (Atomic Force Microscope). The height of the lath magnetite (40 nm for sample-1, 50 nm for sample-2 and 100 nm for sample-3) was roughly proportional to the original thickness of carbon. **Figure 17** shows the result of AFM measurement of one of the lath magnetite formed in the sample-3 (carbon thickness was 300 nm). The cross sectional view of the lath magnetite was clearly observed, whose height was about 119 nm and the width was about 1 100 nm. In addition to the relationship of crystallographic orientation, the macroscopic mechanism of the formation of magnetite from hematite will be very important. The study will be continued on the mechanism of the macroscopic formation of magnetite and be published in present journal.

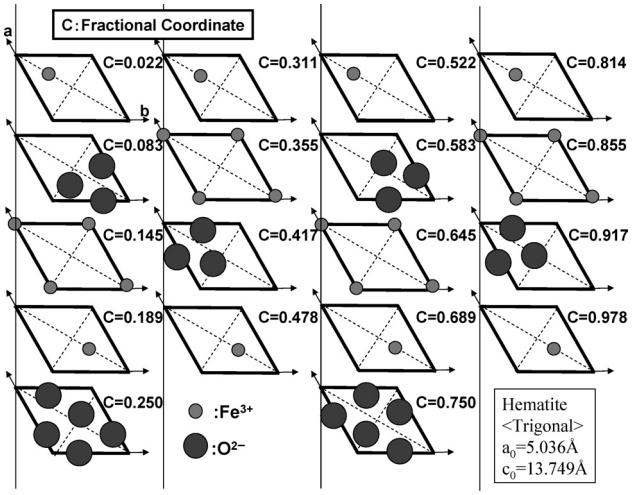

Fig. 13. {001} planes of hematite and Fe and O alignment.

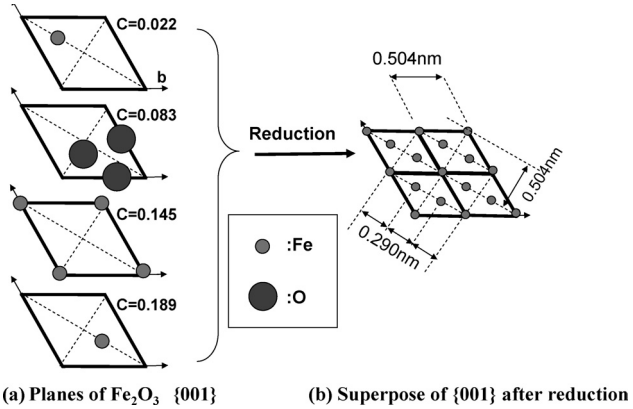

Fig. 14. Transformation of {001} hematite into magnetite in the course of reduction.

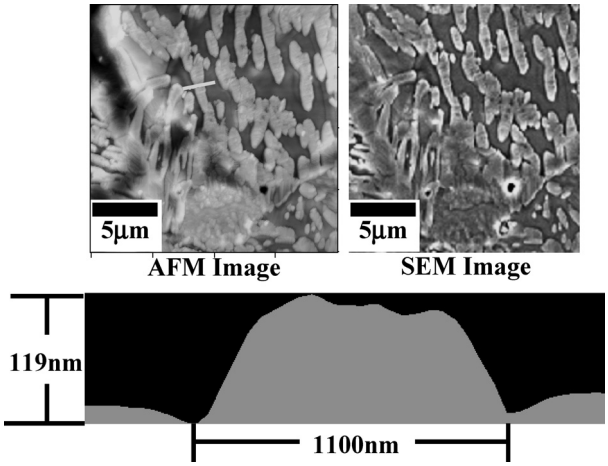

Fig. 17. Results of AFM (Image and topographic profile) and SEM image of the lath magnetite formed after experiment (300 nm).

4. Conclusions

Direct reduction between solid carbon and hematite was investigated by laser microscope equipped with IR furnace.

And crystallographic orientation was clarified by means of EBSP analysis. Following results were obtained.

(1) The direct reduction began from about 650°C and the reduction proceeded rapidly until carbon was consumed. The behavior of reduction was different from the thickness of carbon layer which was related to whether the product gas (CO) could be passed through the carbon layer or not.

(2) After reduction, the lath magnetite having same direction in a grain was observed on the surface.

(3) The crystallographic orientation between magnetite and hematite obtained was as follows;

$$(0\,0\,0\,1)_{H} \parallel (1\,1\,1)_{M}$$
$$[1\,\bar{1}\,0\,0]_{H} \parallel [1\bar{1}0]_{M}$$

(4) The growth direction of the lath magnetite formed on the hematite surface was

$$[2\,1\,\bar{3}\,0]_{H} \parallel [10\bar{1}]_{M}$$

Acknowledgment

We would like to express a deep appreciation to Dr. S. Miura in Graduate school of Materials Science and Engineering, Hokkaido University for assisting us to use the laser microscope.

REFERENCES

1) Y. Kashiwaya, H. Suzuki and K. Ishii: *ISIJ Int.*, **44** (2004), 1970.
2) Y. Kashiwaya, H. Suzuki and K. Ishii: *ISIJ Int.*, **44** (2004), 1975.
3) Y. Kashiwaya and K. Ishii: *ISIJ Int.*, **44** (2004), 1981.
4) Y. Kashiwaya, M. Kanbe and K. Shii: *ISIJ Int.*, **41** (2001), 818.
5) J. R. Porter and P. R. Swann: *Ironmaking Steelmaking*, **24** (1997), 300.
6) P. R. Swann and N. J. Tighe: *Metall. Trans. B*, **8B** (1977), 479.
7) J. Janowski, M. Wyderko-Delekta, A. Sadowski and J. Delekta: *Steel Res.*, **66** (1995), 135.
8) P. C. Hayes and P. Grieveson: *Metall. Trans. B*, **12B** (1981), 579.
9) R. L. Withers and L. A. Bursill: *J. Appl. Cryst.* **13** (1980), 346.
10) Y. Watanabe, S. Takemura, Y. Kashiwaya and K. Ishii: *J. Phys. D, Appl. Phys.* **29** (1996), 8.
11) A. V. Bradshaw and A. G. Matyas: *Metall. Trans. B*, **7B** (1976), 81.
12) J. Janowski and A. Sadowski: *Ironmaking Steelmaking*, **23** (1996), 479.
13) M. Et-Tabirow, B. Dupré and C. Gleitzer: *Metall. Trans. B*, **19B** (1988), 311.
14) J. Janowski, A. Barański and A. Sadowski: *ISIJ Int.*, **36** (1996), 269.
15) H. Brill-Edwards, Dip. Tech., B. L. Daniell, Ph.D., F.I.M. and R. L. Samuel: *J. Iron Steel. Inst.*, **203** (1965), 361.
16) R. Chaigneau and R. H. Heerema: *Metall. Trans. B*, **22B** (1991), 503.
17) H. Hamaguchi and A. Hirakawa: Raman Spectroscopy, Nihon Bunkō gakkai, Tokyo, (1994), 180.